An Investigation of the Application of Taylor's Hypothesis to Atmospheric Boundary Layer Turbulence[1]

DAVID C. POWELL AND C. E. ELDERKIN

Atmospheric Sciences Dept., Battelle, Pacific Northwest Laboratories, Richland, Wash. 99352

(Manuscript received 11 August 1972, in revised form 2 January 1974)

ABSTRACT

The application of Taylor's hypothesis to atmospheric boundary layer turbulence at heights of 15, 30 and 58 m has been investigated by correlation analysis and phase-spectral analysis of data taken from lines of meteorological towers when the mean wind direction was essentially along the tower line. The time lag of maximum cross correlation between parallel components measured at different alongwind locations indicates that the eddy structure travels slightly faster than the mean value of the longitudinal wind at the same height. The autocorrelation functions in space and in time for the longitudinal and vertical components show good agreement, as predicted by Talyor's hypothesis, for space lags up to 252 m. The agreement for the lateral component is inferior for lags $\geqslant 32$ m.

According to Lin, Taylor's hypothesis holds in boundary layer shear flow for those wavenumbers κ such that $\kappa\bar{U} \gg d\bar{U}/dz$. Phase spectral analysis of parallel wind component data at different alongwind locations shows Taylor's hypothesis to hold for $\kappa\bar{U} \geqslant 4d\bar{U}/dz$ for near-neutral turbulence.

Preliminary coherency analysis of the same data indicates that the coherency (not squared) for parallel components falls to a value of less than e^{-1} for wavelengths less than three-halves the separation distance between measuring points.

1. Introduction

According to Lin (1953), the vertical shear of the mean wind in the boundary layer places an upper limit to the wavelengths to which Taylor's hypothesis, equating time correlations and space correlations in turbulence, applies. The primary purpose of this paper is to evaluate the upper wavelength limit by analysis of field data taken from a line of turbulence sensors, logarithmically spaced in the approximate direction of the mean wind in the atmospheric boundary layer. The longer separation distances were on the upwind direction of the line. The four upwind positions were instrumented by Gill anemometers, and the three downwind positions, spanning the shortest separation distances, were instrumented by sonic anemometers.

2. Theoretical framework

Consider a regime of wind tunnel turbulence for which the mean advective velocity is $\bar{U}$ and for which the characteristic turbulence velocity is $\hat{u}$. Taylor's hypothesis (see Taylor, 1938) predicts that if the ratio $\hat{u}/\bar{U}$ is small, the covariance functions of the turbulence in time at a fixed location and in space in the longitudinal direction are, to a good approximation, the same function and may be written

$$\tilde{R}_{ij}(\tau)=\tilde{R}_{ij}(\xi), \quad \xi=\bar{U}\tau; \quad i=1, 2, 3, \quad j=1, 2, 3. \quad (1)$$

In (1) τ is time lag, ξ space lag, and the two covariance tensors are unnormalized.

According to Lin (1953), there is no justification, in general, for extending Taylor's hypothesis to shear flow, such as is found in the atmospheric boundary layer. However, Lin goes on to say that Taylor's hypothesis may still be a good approximation for those wavenumbers κ of the turbulence such that

$$\frac{\kappa\bar{U}}{d\bar{U}/dz} \gg 1 \quad (2)$$

holds. The corresponding equation using frequency rather than wavenumber is

$$\frac{2\pi n}{d\bar{U}/dz} \gg 1, \quad (3)$$

where n is cyclic frequency.

It is desirable to ascertain in what manner this expression is supported by analysis of field data taken in the surface boundary layer.

3. Site description, instrumentation and field array

The area of the U. S. Atomic Energy Commission's (AEC) Hanford reservation over which the measure-

[1] This paper is based on work performed under U. S. Air Force Contract F33615-M-5009 and U. S. Atomic Energy Commission Contract AT(45-1)-1830.

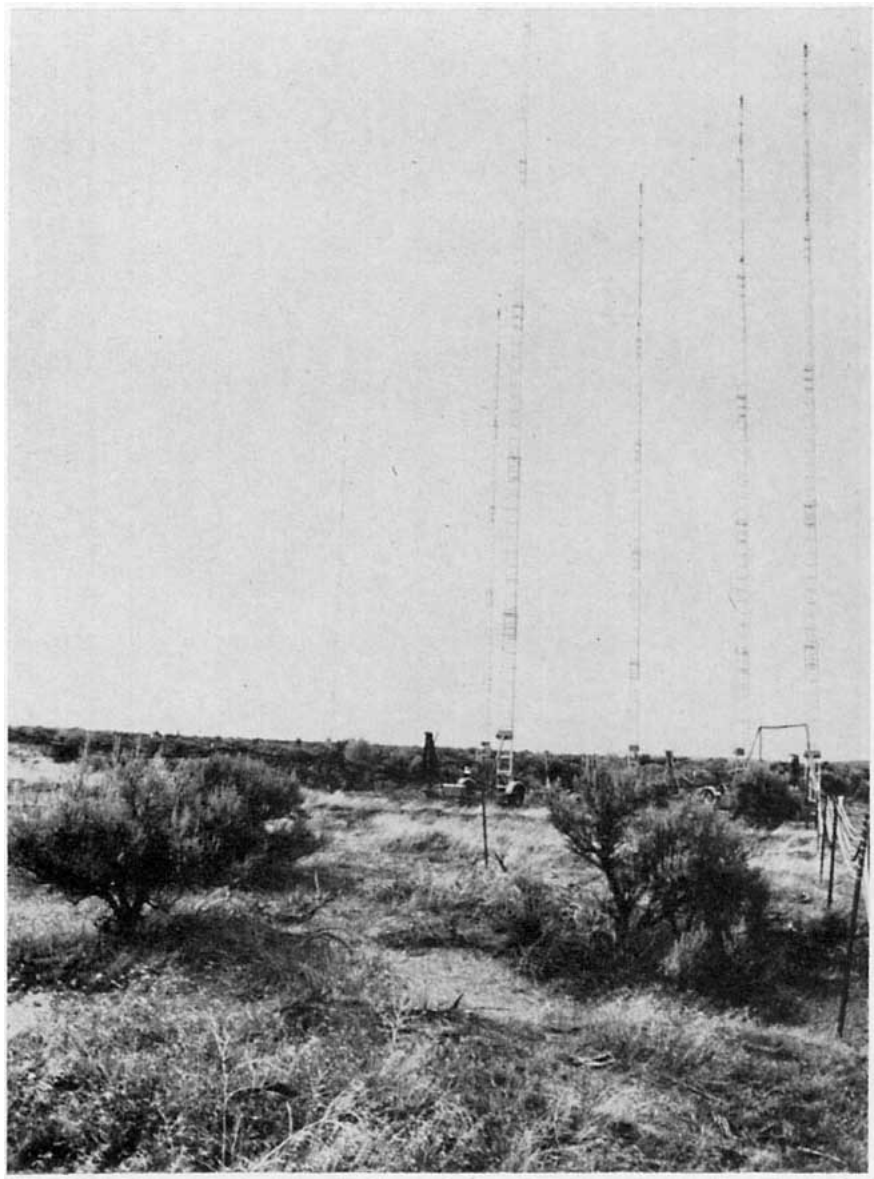

FIG. 1. Measurement array.

ment array was dispersed had relatively uniform vegetative cover and fairly flat terrain. The surface was covered primarily with sagebrush about 1 m in height, moderately dense, and characterized by a roughness length of ~3 cm. The terrain varied in elevation no more than 5 m over the 252 m extent of the array and no more than 30 m for an additional 7 km upwind or 2 km crosswind over the array.

The elevation at the site is about 225 m. Within 16 km of the site hills rise to 600 m in the upwind direction and to 1100 m in the crosswind direction.

Supporting meteorological data are provided by the 400-ft meteorological tower operating continuously at the site. Wind speed and direction, temperature and humidity are measured at the surface and at 50-ft intervals on the tower.

The multi-point turbulence measurement system, providing the data for this study, utilized three-component wind sensors mounted on an array of towers. Turbulence fluctuations in the three components of the wind were measured at various heights and horizontal spacings, and under various meteorological conditions. The measurement array is shown in Fig. 1. The data were collected in the field on analog recorders, played back into a medium-range computer for preprocessing the data, and were re-recorded on industry standard tapes for later detailed processing and analysis on a UNIVAC 1108 computer.

Two types of turbulence sensors were utilized. Fast-response sonic anemometers were used for determination of the friction velocity u_* and the spatial correlations over small separation distances. Less expensive

Gill UVW three-propellor anemometers were used for the greater number of measurements at large separation distances where their slower response was adequate.

Mountings for both types of instruments were located on tower tops and on the ends of tower booms, and were constructed in a manner to assure true sensor leveling and optimum orientation into the wind. This was accomplished by utilizing remotely monitored electrolytic levelers on each sensor and an antenna rotor base on each sensor for remote orientation from centrally located control trailers.

The sensors were mounted on four permanently erected 62 m towers and eight 30 m expandable portable towers which could be repositioned for various measurement configurations to meet different experiment requirements. The sensor booms could be moved to various heights on the 62 m towers, and the sensors on the tops of the 30 m towers could be raised and lowered to measure the turbulence at selected heights.

The two control trailers, downwind of the tower array, contained the signal conditioning and data recording equipment. Two 14-channel, analog, magnetic tape recorders were generally used to record the three wind component signals from each of three sonic anemometers and five Gill anemometers, as well as the temperature signals from each of two sonics. One channel on each recorder was used for a coordination timing signal.

For the experiment to be discussed in greatest detail, data from seven of the sensors were utilized in the analysis. The sensors were located on the expandable towers adjusted to 15 m height and logarithmically spaced along the mean wind direction at 128, 64 32, 16, 8 and 4 m separations between consecutive sensors.

4. Data preparation and analysis

a. Creation of the digital data

The analog data were digitized at the rate of 200 data points per second per parameter. These data were subjected to preliminary editing and were averaged together ten at a time to create digital data at the rate of 20 sec^{-1}.

A more refined editing procedure was imposed on the data as follows. Each set of successive data points for each variable was checked with respect to an arbitrary tolerance T_e, usually set at 3 m sec^{-1} for velocities V. If two successive data points differ by more than T_e, i.e., if

$$|V(t)-V(t-\Delta t)|>T_e, \tag{4}$$

one of three types of editing was employed:

TYPE A. $V(t)$ was set equal to $V(t-\Delta t)$ unless one of the following two conditions applied.

TYPE B. If $|V(t)-V(t-2\Delta t)|\leqslant 0.5\,T_e$, (5)

$V(t)$ was left unchanged and $V(t-\Delta t)$ was set equal to the arithmetic mean of $V(t)$ and $V(t-2\Delta t)$.

TYPE C. If Type B editing was not performed and if

$$|V(t)-V(t+\Delta t)|+|V(t+\Delta t) -V(t+2\Delta t)|\leqslant 0.5\,T_e, \tag{6}$$

no data values were changed, but a notation describing the data discontinuity was printed out, as was done also for Type A and Type B editing.

The subroutine also maintains a count of the data changes, which was printed out for each channel at the conclusion of the tape creation so that the quality of the data may be assessed. The edited Gill anemometer data were also corrected for non-cosine response (Horst, 1973).

b. The method of spectral analysis

Fast-Fourier spectral analysis treats two real data series simultaneously as the real and imaginary parts of a complex data series. The length of each original series must be 2^m points where m is an integer not greater than 13. This allowance of 8192 data per series yields a series of approximately 7 min when Δt is 0.05 sec. Samples of 14, 28 and 55 min may be analyzed by block averaging the original data, 2, 4 or 8 points at a time.

Each of the two data series was subjected independently to a detrending subroutine and then the ends of each series were tapered to zero by using a sine-squared function. For each series the detrending calculates the best-fitting second-order polynomial, subtracts it from the data, and prints out the coefficients. The taper is applied to the 5% at each end of the detrended series.

Mean values for each series, computed before the detrending, were printed out. Also all variances and covariances computed both before and after detrending were printed out.

The fast-Fourier subroutine transforms the 2^m complex data points into 2^m complex Fourier coefficients. These coefficients are appropriately sorted and manipulated to yield 2^{m-1} power spectral coefficients for each of the two real data series and 2^{m-1} complex cross-spectral coefficients related to the two series. From these coefficients, banded estimates are formed for the two power spectra, the cospectrum, and the quadrature spectrum by appropriate summing for 32 logarithmically spaced frequencies. The highest frequency for which estimation is made is the Nyquist frequency N. There are ten estimates per frequency decade; therefore, the lowest frequency for which estimation is made is approximately $N/1259$.

Following these calculations the coherency and phase spectral estimates are made for each frequency band according to

$$\text{Coh}(n)=\left[\frac{\text{Co}^2(n)+Q^2(n)}{S_1(n)S_2(n)}\right]^{\frac{1}{2}}, \tag{7}$$

TABLE 1. Characteristic description of the data.

	Test number T603	T703	T105
Date of recording	19 January 1971	24 March 1971	2 December 1968
Time of recording (PST)	1323–1351	0944–1012	1345–1426
Averaging interval (sec)	0.2	0.2	0.3
Height (m)	15	30	58
Azimuth angle (deg)	9	11	4
$\bar{U}(z)$ (m sec^{-1})	6.4	7.1	8.3
$u_*=[-\overline{uw}(z)]^{\frac{1}{2}}$ (m sec^{-1})	0.46	0.39	0.41
$d\bar{U}/dz$ (sec^{-1})	0.086	0.017	0.021
u_*/kz (sec^{-1})	0.078	0.032	0.018
$\sigma_u/\bar{U}$	0.17	0.10	0.14
$\sigma_v/\bar{U}$	0.12	0.13	0.11
$\sigma_w/\bar{U}$	0.09	0.09	0.09
$u_*/\bar{U}$	0.07	0.05	0.05
z/L	0.05	−1.23	0.32

$$\phi(n)=\tan^{-1}\left[\frac{Q(n)}{\mathrm{Co}(n)}\right], \tag{8}$$

where n is frequency, $\mathrm{Coh}(n)$ is a coherency spectral estimate, and $\phi(n)$ the phase spectral estimate, $\mathrm{Co}(n)$ is a cospectral estimate, $Q(n)$ a quadrature spectral estimate, and $S_1(n)$ and $S_2(n)$ are the two power spectral estimates, all at frequency n.

If the unbanded estimates were used, the coherency spectrum would necessarily be unity for each of the 2^{m-1} frequencies as explained by Jenkins and Watts (1968). However, positive and negative coefficients may be summed to form the banded cospectral estimates and to form the banded quadrature-spectral estimates, thus reducing the coherency spectral values such that the following summation, which derives from a result by Pielke and Panofsky (1970) is satisfied:

$$R(\tau=d/\bar{U}) = \Delta \ln(n) \sum_n \{[nF_1(n)][nF_2(n)]\}^{\frac{1}{2}} \mathrm{Coh}(n), \tag{9}$$

where the cross-correlation value on the left is for the advective time between the two positions, and the functions $F_1(n)$ and $F_2(n)$ are the normalized power spectra for the two locations.

5. Characteristic description of the data

Specifics regarding the three tests analyzed are given in Table 1. The turbulence fluctuations u', v', w' are in the alongwind, crosswind and vertical directions, respectively, and u_*, the friction velocity, is assumed to be the characteristic velocity of the turbulence. When stress is measured at 15 or 30 m, this assumption is more reasonable than when the stress is measured at 58 m, which results in a value that is somewhat low as a characteristic velocity for the turbulence at that height. The k in the table is von Kármán's constant, taken as 0.4. The azimuth angle is the angle between the direction defined by the sensor line and the mean wind direction. The sigma values are the root-mean-square values of the turbulence components, u', v', w'. The L is the Monin-Obuhkov stability length (Lumley and Panofsky, 1964).

The values for $d\bar{U}/dz$ were obtained by differentiating second-order polynomials in $\ln z$ using data from the four lowest measuring levels on the 400-ft Hanford Meteorological Tower. Values for the change of potential temperature with height were obtained similarly from the tower temperature data. From these gradients the gradient Richardson numbers applying to the height of measurement were computed and thence the values of z/L appearing in Table 1.

6. Supporting data analysis

Before evaluating the space and time interrelationships, it will be useful to describe some of the more conventional properties of the turbulence analyzed and to comment on any irregular aspects of the data. First, a comparison of averages and moments under the same conditions and at the same heights will be made. The numerical differences in such a comparison must be indicative of either nonhomogeneity of the site or of differences in instrumental performance. The largest differences shown in the tables below are believed to be of the latter origin since, during subsequent maintenance and calibration, one propeller of the Gill anemometer at position 3 required a bearing replacement, and a zero drift had occurred in the sonic anemometer at position 6.

Such data for test T603 are shown in Table 2. The variances and the momentum flux covariance are given both for unfiltered data and for the same data after a 300-sec running mean was subtracted out.

If the figures from the third and sixth positions are excluded, the values of $\bar{U}$ agree within 0.31 m sec^{-1}, and the values of azimuth angle agree within 5°. The average values given for $\bar{U}$ and α in Table 1 are the averages of the five anemometers that were in relative agreement.

The variances and the stress coveriance are given both for the unfiltered data and for the data as it

TABLE 2. Comparison analysis by position: Test T603.

Parameter	Position Units	1	2	3	4	5	6	7	Average
			Gill anemometer				Sonic anemometer		
$\bar{U}$	(m sec^{-1})	6.48	6.23	5.71	6.48	6.54	5.97	6.42	6.4
α	(deg)	−11.4	−8.3	−1.5	−7.2	−11.4	−6.1	−6.8	−9.0
σ_u^2	(m sec^{-1})^2	1.36	1.41	1.48	1.66	1.80	1.85	1.97	1.65
σ_v^2	(m sec^{-1})^2	0.57	0.66	0.54	0.67	0.77	0.78	0.76	0.68
σ_w^2	(m sec^{-1})^2	0.34	0.32	0.36	0.39	0.37	0.36	0.33	0.35
$-\overline{uw}$	(m sec^{-1})^2	0.19	0.20	0.18	0.22	0.24	0.23	0.23	0.21
				Filtered data*					
σ_u^2	(m sec^{-1})^2	1.12	1.13	1.04	1.24	1.26	1.32	1.41	1.22
σ_v^2	(m sec^{-1})^2	0.48	0.54	0.41	0.53	0.63	0.64	0.61	0.55
σ_w^2	(m sec^{-1})^2	0.33	0.30	0.34	0.37	0.35	0.35	0.32	0.34
$-\overline{uw}$	(m sec^{-1})^2	0.20	0.22	0.17	0.21	0.21	0.23	0.22	0.21

* 300-sec high-pass filter used.
Notes: All second moments are in a coordinate system oriented with the mean wind direction; average $\bar{U}$ and average α are from positions 1, 2, 4, 5, 7; average second moments are from all data.

emerged from a 300-sec high-pass filter. The significant reduction of the horizontal variances by the filtering is apparent, as well as the lack of similar reduction of the vertical variances and the stress covariance. As expected, the second-moment statistics from the Gill anemometers show lesser values than do the sonic statistics because of the poorer response. Similar data are given for test T703 in Table 3 and for test T105 in Table 4.

It is believed that the magnitude differences, being primarily differences in sensor performance, do not significantly affect the phase spectral analysis and coherency analysis given in Section 8.

Specifically, the cross analyses from test T603 employing data from the third or sixth positions were found to be in agreement with and as well organized as other cross analyses from the same test.

The turbulence recorded during test T603, which is analyzed in greater detail than either of the other two tests, is not exceptionally stationary. The mean quantities and second moments for each of four 7-min periods are given below in Table 5. Since the nonstationarity may affect the interpretation of the principal results, the succeeding 28-min period of the same test, which was more stationary, was also analyzed. Results are compared in Section 9.

The normalized logarithmic power spectra for test T603 are given in Fig. 2. The spectra are uncorrected and unsmoothed except for the banding described in Section 4. The spectra show the expected inertial subrange slope of $\frac{2}{3}$ and some tendency of the spectral values of the two lateral components to exceed the values for the horizontal component. The power spectrum for w' matches reasonably well a model for other Hanford w' spectra in neutral conditions, as given by Elderkin *et al.* (1971):

$$\frac{nS_w(n)}{u_*^2}=\frac{1.15(f/0.46)}{1+1.5(f/0.46)^{5/3}}, \tag{10}$$

where

$$f=nz/\bar{U}. \tag{11}$$

This model is in good agreement with those proposed by other investigators. Busch and Panofsky (1968) propose an expression of exactly the same form with 1.075 as the constant in the numerator and 0.32 as the denominator for f. However, their value of 0.32 is for neutral and unstable conditions, an average of which necessitates the use of a lower normalizing figure for f than that which applies to neutral conditions. Kaimal *et al.* (1972) give an expression which, when converted

TABLE 3. Comparison analysis by position: Test T703.

Parameter	Position Units	1	2	3	4	Average
			Gill anemometer			
$\bar{U}$	(m sec^{-1})	6.77	7.51	6.65	7.55	7.12
α	(deg)	−13.8	−12.7	−7.0	−8.9	−10.6
σ_u^2	(m sec^{-1})^2	0.73	0.74	0.50	0.68	0.66
σ_v^2	(m sec^{-1})^2	0.76	1.03	0.70	0.78	0.82
σ_w^2	(m sec^{-1})^2	0.48	0.49	0.30	0.36	0.41
$-\overline{uw}$	(m sec^{-1})^2	0.18	0.26	0.13	0.15	0.18
			Filtered data			
σ_u^2	(m sec^{-1})^2	0.55	0.59	0.38	0.49	0.50
σ_v^2	(m sec^{-1})^2	0.46	0.57	0.41	0.43	0.47
σ_w^2	(m sec^{-1})^2	0.41	0.44	0.28	0.33	0.37
$-\overline{uw}$	(m sec^{-1})^2	0.15	0.21	0.10	0.12	0.15

TABLE 4. Comparison analysis by position: Test T105.

Parameter	Position Units	Tower 122	Tower 114	Average
		Sonic anemometer		
$\bar{U}$	(m sec^{-1})	8.41	8.06	8.24
α	(deg)	−3.6	−4.2	−3.9
σ_u^2	(m sec^{-1})^2	1.39	1.34	1.36
σ_v^2	(m sec^{-1})^2	1.27	1.36	1.32
σ_w^2	(m sec^{-1})^2	0.69	0.51	0.60
$-\overline{uw}$	(m sec^{-1})^2		0.177	0.18
		Filtered data		
σ_u^2	(m sec^{-1})^2	1.32	1.26	1.29
σ_v^2	(m sec^{-1})^2	0.84	0.91	0.88
σ_w^2	(m sec^{-1})^2	0.70	0.53	0.61

TABLE 5. Comparison analysis by time period (one sonic anemometer): Test T603.*

Parameter	Minutes 1–7	8–14	15–21	22–28
$\bar{U}$	5.66	6.45	6.34	7.60
α	−11.5	−9.3	−13.7	−11.9
σ_u^2	0.88	1.43	1.26	1.90
σ_v^2	0.87	0.71	0.54	1.03
σ_w^2	0.43	0.35	0.36	0.46
$-\overline{uw}$	0.27	0.24	0.23	0.16
	Filtered data			
σ_u^2	0.87	0.74	1.22	1.47
σ_v^2	0.70	0.65	0.46	0.82
σ_w^2	0.46	0.31	0.38	0.46
$-\overline{uw}$	0.30	0.17	0.27	0.17

* See Tables 2–4 for units.

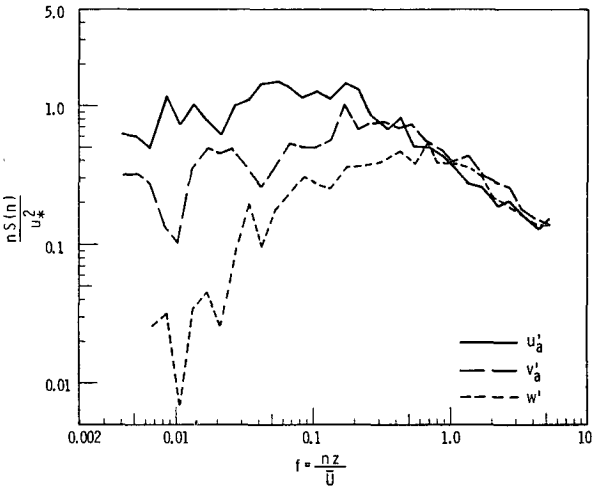

FIG. 2. Dimensionless power spectra.

to the form of Eq. (10), has a numerator constant of 0.94 and a normalizing figure of 0.47 for f. It is considered that the comparisons made above demonstrate that the quality and representativeness of the data are sufficient to warrant investigation of the spatial correlations and cross-spectral analyses of the data.

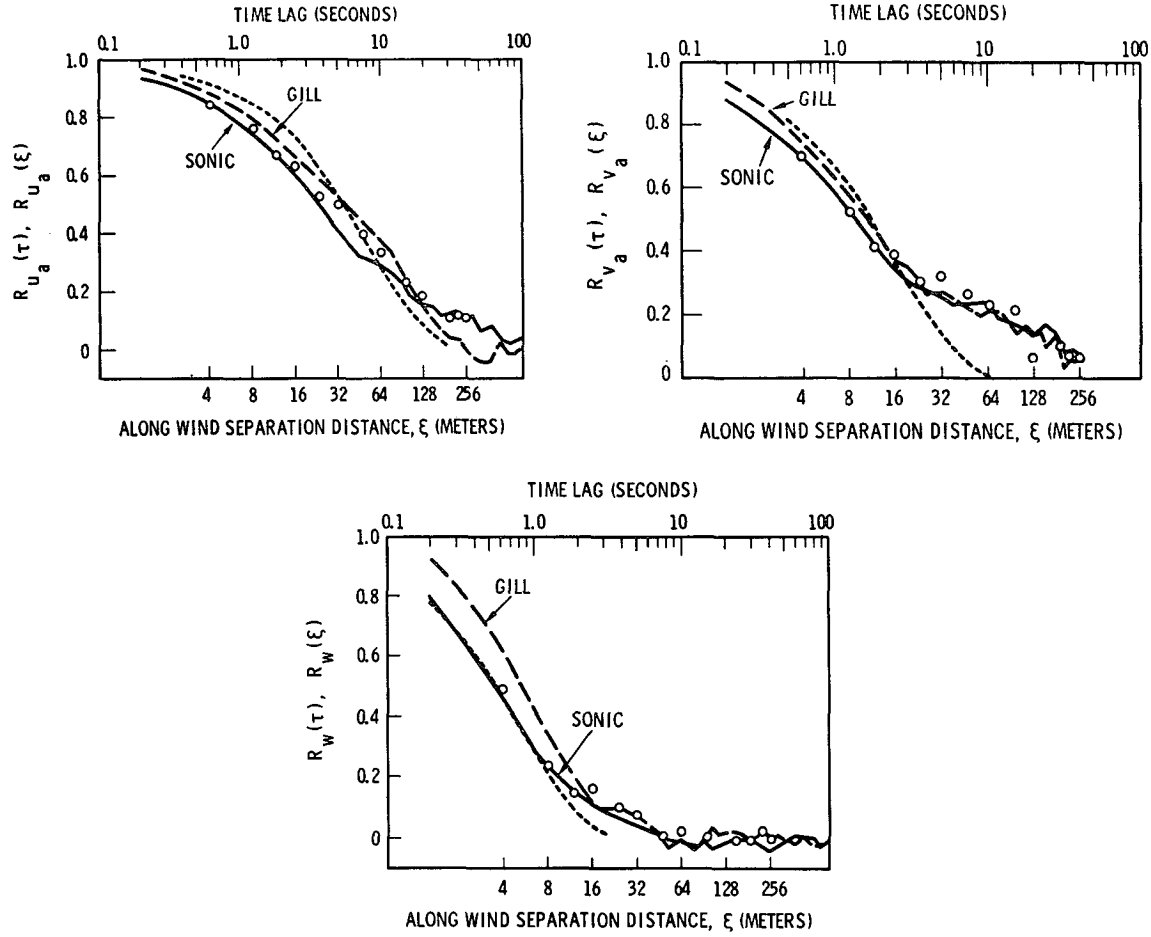

FIG. 3. Comparison of the time correlations and space correlations for each of the three turbulence components of test T603.

7. Correlation analysis

Each set of two towers in the logarithmic array was separated by a unique distance. Therefore, genuine spatial covariances, computed by averaging over space, were not available. Instead, the pseudo-spatial covariances were computed by averaging over time the products of winds for two points in space. Because of the arrangement of sonic and Gill anemometers in the array, the space correlations at 4, 8 and 12 m were computed using data from sonic anemometers; the space correlations at 32, 64, 96, 128, 192 and 224 m were computed using data from Gill anemometers; and the space correlations at 16, 24, 48 and 252 m were computed using data from one sonic and one Gill. The notation for the components of the wind parallel and lateral to the tower line is u_a' and v_a'. The corresponding autocorrelation functions are R_{u_a} and R_{v_a}.

Comparison of the time correlations and space correlations for each of the three turbulence components of test T603 is shown in Fig. 3. Each of these graphs exhibits four correlation functions, utilizing two scales for the abscissa and one scale for the ordinate. The four correlation functions are: 1) solid line, time autocorrelation from sonic data; 2) dashed line, time autocorrelation from Gill data; 3) large dots, spatial correlations; and 4) dotted line, the exponential function

$$R(\xi)=\exp(-\xi/L_0),$$

with L_0 so determined that the exponential function matches the spatial autocorrelation where the value is e^{-1}.

The scale for the abscissa along the top of each figure is for time lag. The scale for the abscissa along the bottom of the figure is for space lag, which is scaled to match the time lag according to Eq. (1). The scale along the ordinate is for the correlation values.

Fig. 3 shows the space correlations and the time correlations comparing almost exactly for all three components for distances up to 12 m and with reasonable proximity all the way out to 252 m. Only the analysis for v_a' shows a number of the space correlation values departing noticeably from the "envelope" between the sonic and Gill time correlations. The departure begins at 32 m.

The exponential model overestimates the correlation at lags shorter than the lag at which the model was fitted and underestimates the correlations at longer lags.

The only data analyzed from test T703 were the Gill data. The azimuth angle for this test was 11° (compared to 9° for test T603), and the conditions were unstable. For u_a' the spatial correlations fell off somewhat more rapidly than the corresponding time correlations but did not deviate by more than the envelope width shown in Fig. 3. For v_a' and w' the correspondence between time and spatial correlations was quite strong in spite of the larger azimuth angle and supports Taylor's hypothesis as did the correlation functions from test T603.

For test T105 there was only one separation distance, 223 m. When the spatial correlations at zero time lag for u_a' and v_a' are plotted against the corresponding time correlation curves at the proper advective lag, the spatial correlation values miss the time correlation curves by less than 0.01. Because the time correlation for w' crossed the zero value for a time lag equal to one-third the advective time between the two positions, no comparison could be made for w'.

The particular functions shown in Fig. 3 cannot be used to determine whether the eddies are being advected at the mean wind speed at the height of measurement or at some other speed, which may be called an eddy translation speed. The ratio of the eddy translation speed to the mean wind speed may be estimated by computing for each separation distance ξ the quantity, $\xi/(\bar{U}\tau_m)$, where τ_m is the time lag of the maximum cross correlation between the parallel components separated by distance ξ. When done for all ξ from 4 to 32 m, the average results for u_a', v_a' and w' were 1.20, 1.11 and 1.16, respectively.

These results cannot be properly interpreted without considering the modified Taylor's hypothesis shown by Heskestad (1965). Assuming isotropic turbulence, Heskestad shows that the first-order equation

$$\overline{\left(\frac{\partial u'}{\partial t}\right)^2}=\bar{U}^2\overline{\left(\frac{\partial u'}{\partial x}\right)^2}, \tag{12}$$

must be modified to read

$$\overline{\left(\frac{\partial u'}{\partial t}\right)^2}=\bar{U}^2\overline{\left(\frac{\partial u'}{\partial x}\right)^2}\left[1+\frac{\sigma_u^2}{\bar{U}^2}+2\frac{\sigma_v^2}{\bar{U}^2}+2\frac{\sigma_w^2}{\bar{U}^2}\right]. \tag{13}$$

For test T603 the variances for u_a', v_a' and w' were 1.65, 0.68 and 0.35 m^2 sec^{-2}, respectively. Inserting these into (13) suggests a correction factor of 10%. Presumably the correction factor applicable to $\bar{U}$ as a translation rate is the square root of the correction for the squares, leaving 4%. Equations similar to (13) may be derived for the other two components, and when evaluated, the correction factor is about 3%. Dividing the translation ratios by these correction factors still leaves eddy translation ratios of 1.15, 1.08 and 1.13 for the three wind components, u_a', v_a' and w', respectively. Thus, the corrected ratios still show the eddies traveling faster than the mean wind speed, which could be estimated nominally within 5%.

TABLE 6. Eddy translation ratios.

Component	Test number T603	T703	T105
u_a'	1.15	1.11	1.05
v_a'	1.08	1.02	1.02
w'	1.13	1.03	1.08

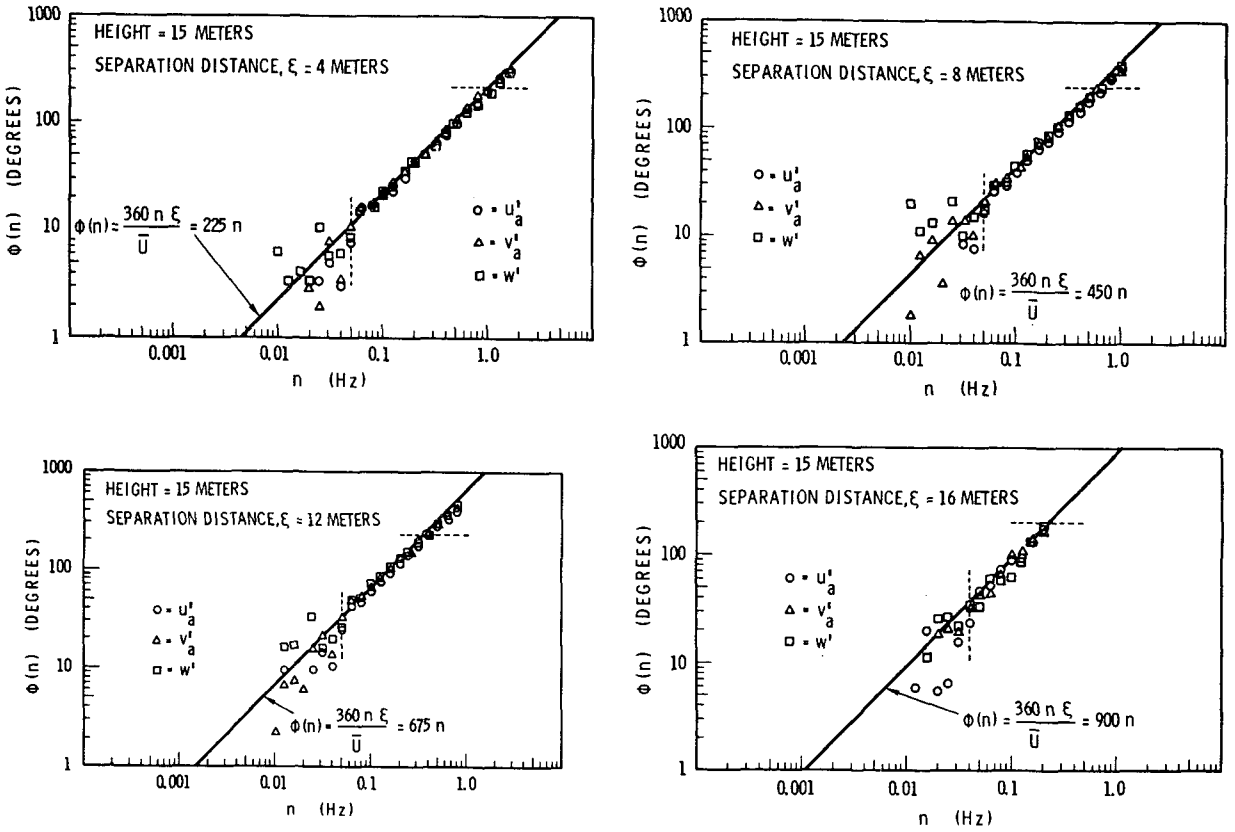

FIG. 4. Phase spectra for separation distances 4 to 16 m: Test T603.

The eddy translation speed again calculated from the time lag for maximum correlation also tends to be generally higher than the mean wind speed for tests T703 and T105. The eddy translation ratios ξ for the three tests and for each component are given in Table 6.

These ratios appear to decrease with height from 15 to 30 m, again suggesting that the eddies at different heights in the boundary layer are advected not according to the mean wind at the height of measurement, but either by a common wind speed or by some weighted average of the mean wind speed at the particular height and a common wind speed.

An eddy translation ratio slightly higher than the mean wind speed has also been noted by Panofsky *et al.* (1973).

8. Phase-spectral analysis

The required data for this type of analysis may be obtained by recording data from at least two sensors, one of which is placed downwind of the other. For these data, if Taylor's hypothesis holds, it would be expected that the phase spectrum calculated by cross analyzing parallel components from both sensors would be

$$\phi(n) = 360 n \xi / \bar{U} \qquad (14)$$

in degrees.

For test T603, data for u'_a, v'_a and w' are available from the entire logarithmic line of seven sensors. The phase-spectral analysis to be presented draws chiefly on the results from this test. Investigation of height dependency is initiated by introducing results from tests T703 and T105, based on analysis of data from fewer sensors.

The results from test T603 can best be seen by examining the set of eight phase-spectral plots as a group (Figs. 4 and 5). There is one graph plotted for each separation distance where phase spectra show any organization. These distances are 4, 8, 12, 16, 24, 32, 48 and 64 m. Items requiring explanation on the graphs are as follows:

1) The heavy diagonal line across each figure is the theoretical phase spectrum predicted by Taylor's hypothesis.

2) The equation of this line [(14)] is given elsewhere on the figure, first in general form and then in final calculated form, using $\bar{U} = 6.4$ m sec^{-1}.

3) The dashed vertical line indicates the lower frequency limit at which the phase spectra for the three components appear organizable.

4) The horizontal dashed line is an upper limit of coherency, the significance of which is discussed below.

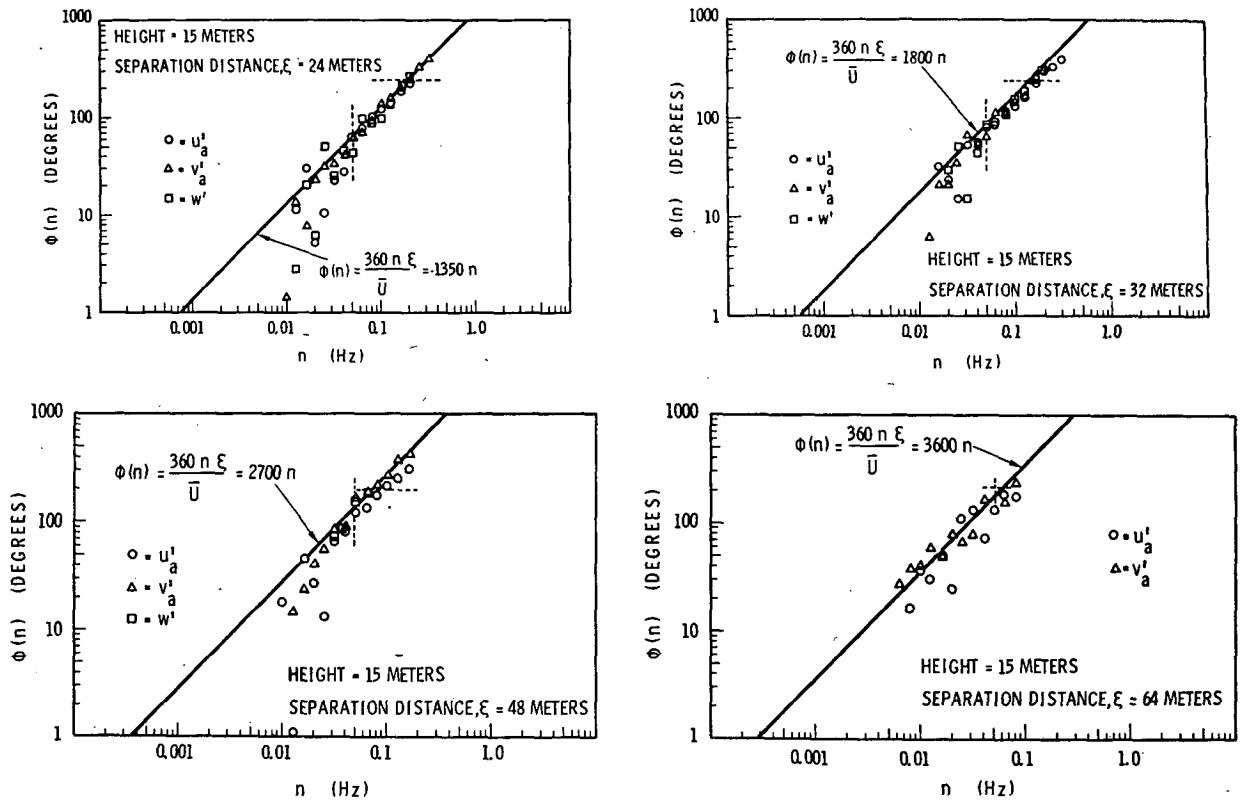

FIG. 5. Phase spectra for separation distances 24 to 64 m: Test T603.

Consider once more the passage of turbulence from the location of one sensor to that of another in the downwind direction. Assume that the sensors are close enough together so that the larger scale variations in the turbulence maintain their characteristics, or individualities, over the path of advection, i.e., this part of the turbulence is coherently advected from one location to the other. Intuitively, there must be a lower limit to the size of the variations that can be coherently advected over the given path and hence an upper limit to the frequencies representing these variations in the time series. This is important in phase-spectral analysis because the phase spectra might not be expected to show organization at frequencies above the upper limit of coherency.

Because the coherency function is continuous, some arbitrary cutoff value of coherency must necessarily be selected before an upper frequency limit can be defined. Although the maximum frequency of eddies considered to be coherently advected will depend on what cutoff value of coherency is arbitrarily chosen, much may be learned from an extended study in which one cutoff value is uniformly applied. The cutoff value adopted for these studies is e^{-1}, or about 0.37. The upper limit of coherency is defined as that frequency of the u'_a spectrum at which the coherency function is e^{-1}. This value was chosen because the slope of the coherency function is usually quite steep through this value.

The best way to gain insight from the phase-spectral graphs (Figs. 4 and 5) is to examine them in sequence in order of increasing separation distance, observing certain changes. As the separation distance increases, the line function for the ideal phase spectrum moves to a higher phase location on each succeeding graph, associating a larger value of the phase angle with the same frequency. Theory predicts that the vertical line, indicating the lowest frequency at which the phase spectrum is organized, should be at the same frequency regardless of separation distance. This frequency, n_0, appears to be reasonably estimated at 0.05 Hz from the analyses. The horizontal line, indicating the upper limit of coherency, appears at approximately the same phase angle ϕ_0 on each diagram. The placement of this upper limit of coherency varies slightly, but not significantly, about 240°, except that for the 16, 48 and 64 m separation distances the line is at about 200°. Phase-spectral data have been plotted above this value where organized results were found. Therefore, as the graphs are viewed in order of increasing separation distance, the diagonal line rises and its intersections with the fixed cutoff for n_0 and ϕ_0 converge, thereby decreasing the portion of the diagonal line that is followed by organized phase-spectral functions. The graphs show 64 m as the separation distance for which the horizontal and vertical lines intersect the diagonal at almost the point of convergence of these intersections. For greater separation distances the phase spectra show

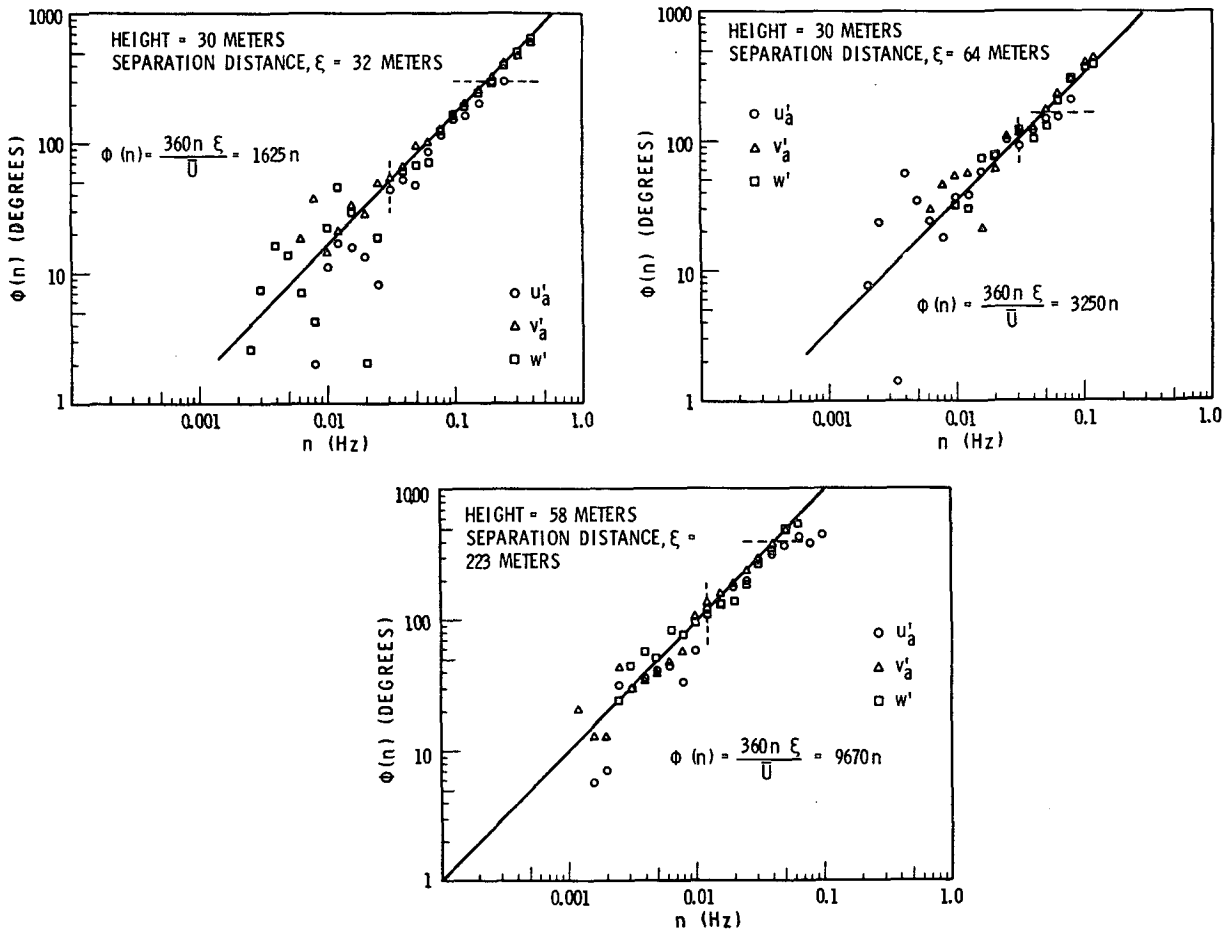

FIG. 6. Phase spectra from tests T703 and T105.

little tendency to correlate with the diagonals. Also for the 64 m separation distances, only the phase spectra of the two horizontal components were well enough organized to constitute functions of frequency. If any of these functions are drawn by connecting consecutive data points for each wind component with straight lines, the difference in behavior between the organized portion contained above n_0 and below ϕ_0, in comparison to the unorganized portion below n_0, is made even more apparent by the extremes of slope variation in the phase spectral function in the unorganized region of low frequency.

The summary of results from the 15 m data is as follows:

1. The phase spectra are organized from a frequency of 0.05 Hz up to or beyond the frequency of the coherency limit. This implies that during this test Taylor's hypothesis was valid for all frequencies above the lower limit, notwithstanding the upper limit of coherency.
2. The frequency limit of coherency was approximately 240° for separation distances up to 32 m. This figure corresponds to a decay factor of 3 for alongwind separations of the longitudinal component in the model proposed by Ropelewski *et al.* (1973). For longer separation distances the decay factor is larger, and this dependency is the subject of continuing investigation.
3. Most of the experimental data points are slightly below the line of the ideal spectrum. This agrees with the previously mentioned indication that the eddies are traveling faster than the mean wind speed.

Phase-spectral and coherency results from tests T703 and T105 are shown in Fig. 6. The two separation distances for which organized phase spectra could be plotted from test T703 show a value of 0.032 Hz for n_0. The one separation distance for which data could be analyzed from test T105 shows a value of 0.012 Hz for n_0.

In view of the different azimuth angles, stabilities, and sampling times for the tests shown in Table 1, any physical inferences about the role of the wind shear must be tentative. The value for n_0 clearly decreases with increased height. On the basis of Lin's hypothesis (see Section 2), the decrease of n_0 with height is a logical

TABLE 7. Comparison by analysis time (one sonic anemometer): Test T603, second 28-min period.

Parameter	Minutes 29–35	36–42	43–49	50–56
$\bar{U}$	7.19	7.11	7.07	7.34
α	−9.4	−10.3	−12.2	−11.0
σ_u^2	1.37	2.14	2.04	1.91
σ_v^2	0.83	0.91	1.14	0.87
σ_w^2	0.44	0.50	0.59	0.45
$-\overline{uw}$	0.20	0.34	0.35	0.24
	Filtered data			
σ_u^2	1.24	1.42	1.48	1.18
σ_v^2	0.76	0.84	1.06	0.73
σ_w^2	0.42	0.47	0.57	0.44
$-\overline{uw}$	0.16	0.23	0.29	0.21

consequence of the decrease of shear with height. However, Table 1 shows that the calculated shear at the height of measurement for the test at 58 m (T105) was not less than the calculated shear at 30 m (T703). Evidently data from more experiments are needed to assess the roles of stability and azimuth angle.

The coherency spectra drop to e^{-1} at different values of the phase spectra for the two separation distances of test T703—300° for the 32 m separation distance and 170° for the 64 m separation distance. The coherency spectrum for test T105 drops to e^{-1} at the frequency where $\phi(n)$ is 340°.

9. Comparisons involving differences of stationarity and calculational methods

Questions may arise regarding how the quoted results would change if more stationary data were analyzed, or if certain variations were made in the computational procedures. In this section the analysis of a more-stationary data segment is summarized, followed by a discussion of the effects of computational variations on the autocorrelation function, the phase spectrum, and the coherency function.

a. Comparison with analysis of more-stationary turbulence

An additional period of 28 min during test T603 was analyzed to assess the influence of the nonstationarity characterizing the first 28 min (see Table 5). The results show no sensitivity to the prevailing nonstationarity for the types of analysis performed. Perhaps this is not surprising since the time lags involved in the cross analysis are short compared to the time scale of the nonstationarity. The mean values and moments for the four 7-min intervals of the second 28-min period are given in Table 7.

For the second period the ratios of the eddy translation speed to the mean wind speed are 1.13, 1.09 and 1.12 for u_a', v_a' and w', compared to 1.15, 1.08 and 1.13 for the first period.

The lower frequency limit n_0 of the organized phase spectra is not as well defined for the second period as for the first. The amount of scatter of the points at $n=0.05$ Hz is about the same for both periods, but there is more scatter at 0.063 and 0.080 Hz for the second period. However, the difference is not great enough to declare a higher value of n_0 for the second period. Also the coherency result quoted for the first period is applicable to the second period.

These findings are important because they suggest that models of cross analysis of turbulence for stationary conditions are also applicable for moderate nonstationarity.

b. Effects of variation of computational procedure on the different functions.

It may be argued that certain mathematical descriptors used in the above analysis, the autocorrelation function, the phase spectrum and the coherency spectrum, may yield significantly different results if a longer or shorter time span of the same data is used or if different banding is used to obtain banded spectral estimates from the estimates for the individual harmonics. To investigate these changes, the analysis of test T603 was extended to a 55-min period, within which two 28-min periods, four 14-min periods and eight 7-min periods could be analyzed with Δt varying proportionally.

For computing the autocorrelation functions, however, the only time period used other than 28 min was 55 min. There is no significant difference overall between these correlation functions and those for the 28-min analysis. The correspondence between the spatial correlations and the time correlations for u_a' is somewhat closer in the 55-min analysis. For v_a' the 55-min analysis again shows the spatial correlation high at 32 and 64 m, and low at 128 m. The integral scales of the correlation functions are not significantly different for the two time periods.

It is noted that the phase-spectral estimates below the frequency n_0 occur randomly above and below the line of the theoretical phase spectrum in most of the graphs. Since there is no consistent indication that the larger eddies travel either slower or faster than the smaller eddies, it is possible that the convergence of the estimates to the theoretical phase spectrum is a purely statistical phenomenon. If so, the convergence for the 7-min analysis should be at a frequency eight times as great as is the convergence frequency for the 55-min analysis.

To compare the phase spectra for different length periods, a means of quantifying the departure at each frequency of the experimental spectra from the theoretical models was devised and applied to the graphs for the 4, 8 and 12 m separation distances. Using the original hand-drawn charts on log-log paper and considering each frequency for which a banded estimate was available, the vertical distances of the three experimental values (one for each of u_a', v_a', w') was considered. On log-log paper these distances are always equivalent

to ratios. For this particular investigation the ratio was always considered to be unity or greater since the lower of the two values, the experimental value or the theoretical value, is placed in the denominator. The largest of the three ratios thus obtained at each frequency was tabulated and called a departure ratio.

The departure ratios were tabulated for the frequencies near n_0 for the different length-analysis periods for the 4, 8 and 12 m separation distances and averaged for each frequency and for each analysis length period. The result is shown in Fig. 7. The abscissas are the departure ratios and the ordinates the frequencies.

If the major part of the slope of the line for the 7-min analysis is compared with the parallel slopes for the 55-min analysis, the frequency ratio between the placement of the two curves is suggested to be between 2 and 4. Thus, when the time scale of the analysis changes eightfold, the lowest frequency at which the phase spectrum shows organization changes not eightfold, but by a ratio that is closer to the square root of eight.

Using 0.05 Hz as a representative value for n_0 and the value of 0.086 $\sec^{-1}$ for $d\bar{U}/dz$ in (3), we find Taylor's hypothesis holding for frequencies such that

$$\frac{2\pi n}{d\bar{U}/dz} \geqslant \frac{2\pi \times 0.05}{0.086} = 3.6. \qquad (15)$$

For lower frequencies the shear prevents dependable correspondence between the temporal variations at one point and the spatial variations along the mean wind direction.

Phase spectral functions were also computed for the 4, 8 and 12 m separation distances with different banding, i.e., with 5 or 20 logarithmically spaced bands per decade instead of 10, using the original 28-min data segment. The organizing frequency n_0 was 0.05 Hz for 5 bands per decade and 0.056 Hz for 20 bands per decade, showing no appreciable effect of banding.

The coherency result quoted earlier is based primarily on coherencies for u_a' measured at separation distances $\leqslant 32$ m. Comparison using the 4, 8 and 12 m separation distances showed no significant difference either when the analysis period was varied from 7 to 55 min or when the banding in the 28-min analysis was doubled or halved. When numerical comparison was made for the different banding, it was found that the coherencies averaged about 0.02 higher when there were 20 logarithmically spaced bands per decade than when there were 5.

However, for the longer separation distances, particularly for separation distances long enough that no organized phase spectrum is found, the coherency value of e^{-1} corresponds to theoretical phase spectral values that are lower than 240° and which decrease as the separation distance increases. Also the change of band width makes significant differences in these coherency functions. The significance of these results is under current investigation.

TABLE 8. Summary of phase-spectral and coherency analysis.

	Test number		
	T603	T703	T105
Height (m)	15	30	58
z/L	0.05	−1.23	0.32
Duration (min)	28	28	41
n_0(Hz)	0.050	0.032	0.012
$\kappa_0\bar{U}/(d\bar{U}/dz)$ (rad)	3.6	11.8	3.6
$\kappa_0\bar{U}/(u_*/kz)$ (rad)	4.0	6.2	4.2
$\lambda_0=\bar{U}/n_0$ (m cycle^{-1})	128	233	692
$\lambda_0/z=(n_0z/\bar{U})^{-1}$	8.5	7.8	11.9
$\xi/\bar{U}\tau_m$ (average value)	1.12	1.05	1.05
ϕ_0 (deg)	240°	—	340°

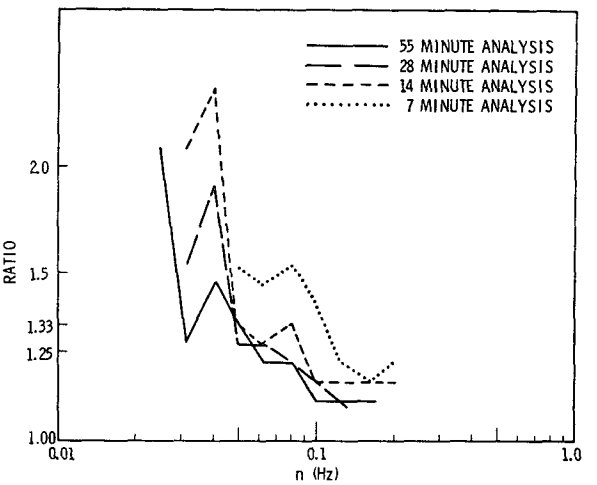

FIG. 7. Departure ratios of phase spectral estimates from theoretical phase spectrum.

10. Summary

Comparison of space and time correlations would suggest Taylor's hypothesis holds quite well. However, correlation analyses do not demonstrate how the hypothesis holds at various wavelengths. Phase and coherency spectral analysis permits wavelength dependency to be investigated.

A summary of the phase-spectral and coherency analysis for the three original test periods is included in Table 8. In the table, $\kappa_0\bar{U}=2\pi n_0$, and ϕ_0 is the theoretical phase evaluated at the frequency where the coherency is e^{-1}.

The following results are apparent from the table.

1. Except for the unstable case, the limitation expressed by Lin on the application of Taylor's hypothesis in (2) is too severe, where for data samples of half an hour to an hour in length, Taylor's hypothesis is found holding for

$$\kappa\bar{U}/(d\bar{U}/dz) \gtrsim 3.6. \qquad (16)$$

2. The waves move at a speed greater than the mean wind speed at the height of measurement. The ratio of the eddy translation speed to the mean wind speed decreases with height from 15 to 30 m.
3. The statistic obtained by dividing $\kappa\bar{U}$ by u_*/kz appears less variable than Lin's expression using $d\bar{U}/dz$ in the denominator. This may be because the lower wavenumber limit to which Taylor's hypothesis applies is a function of both shear and stability. In the specific unstable case at 30 m, the instability makes the quotient formed by dividing the turbulence characteristic velocity by the height larger compared to $d\bar{U}/dz$ than would be the case in neutral conditions. It may be that the physical criterion limiting the application of Taylor's hypothesis to low wavenumbers is the turbulence characteristic velocity rather than the wind shear.
4. The wavelengths corresponding to the frequency n_0 are roughly ten times the height of measurement.
5. If a value of e^{-1} is accepted as a lower limit of coherency, eddies are coherently advected over paths not greater than their alongwind dimension.

From earlier discussion the following may be summarized:

1) Phase-spectral and coherency analysis of two consecutive 28-min periods differing markedly in stationarity shows no differences that can be attributed to the difference in stationarity.

2) The lowest frequency (n_0) at which organized phase spectra occur in the analysis for the 4, 8 and 12 m separation distances varies by a factor of 2 to 4 as the sampling time and sampling interval are varied eightfold from 7 to 55 min, with the number of data in each sample held constant at 8192.

3) The coherency analysis of the same data shows little change.

Acknowledgment. The measurement system was developed by Mr. A. G. Dunbar.

REFERENCES

Busch, N. E., and H. A. Panofsky, 1968: Recent spectra of atmospheric turbulence. *Quart. J. Roy. Meteor. Soc.*, **94**, 132–148.

Elderkin, C. E., D. C. Powell and T. W. Horst, 1971: Modeling of wind component spectra. Annual Report for 1970, BNWL-1551, Vol. II, Part 1, Battelle, Pacific Northwest Laboratories, Richland, Wash., 148–153.

Heskestad, G., 1965: A generalized Taylor hypothesis with applications for high Reynolds number turbulent shear flows. *J. Appl. Mech.*, **87**, 735–739.

Horst, T. W., 1973: Corrections for response errors in a three-component propeller anemometer. *J. Appl. Meteor.*, **12**, 716–725.

Jenkins, G. M., and D. G. Watts, 1968: *Spectral Analysis and its Applications*. San Francisco, Holden-Day, 525 pp.

Kaimal, J. C., J. C. Wyngaard, Y. Izumi and O. R. Coté, 1972: Spectral characteristics of surface layer turbulence. *Quart. J. Roy. Meteor. Soc.*, **98**, 563–589.

Lin, C. C., 1953: On Taylor's hypothesis and the acceleration terms in the Navier-Stokes equation. *Quart. Appl. Math.*, **10** 294–306.

Lumley, J. L., and H. A. Panofsky, 1964: *The Structure of Atmospheric Turbulence*. New York, Wiley, 239 pp.

Panofsky, H. A., D. Sullivan, D. W. Thomson and D. Moravek, 1973: Coherence between wind speed fluctuations over Lake Ontario. *Preprints Third Conf. Probability and Statistics in Atmospheric Science*, Boulder, Colo., Amer. Meteor. Soc., 274–276.

Pielke, R. A., and H. A. Panofsky, 1970: Turbulence characteristics along several towers. *Boundary Layer Meteor.*, **1**, 115–130.

Ropelewski, C. F., H. Tennekes and H. A. Panofsky, 1973: Horizontal coherence of wind fluctuations. *Boundary Layer Meteor.*, **5**, 353–363.

Taylor, G. I., 1938: The spectrum of turbulence. *Proc. Roy. Soc. London*, **A165**, 476–484.